Direct, Absolute, and *In Situ* Measurement of Fast Electron Transport via Cherenkov Emission

Hideaki Habara, Kazuhide Ohta, and Kazuo A. Tanaka
Graduate School of Engineering, Osaka University, 2-1 Suita, 565-0871, Osaka, Japan

G. Ravindra Kumar, M. Krishnamurthy, Subhendu Kahaly,* Sudipta Mondal, Manoj Kumar Bhuyan, and R. Rajeev
Tata Institute of Fundamental Research, Homi Bhabha Road, Mumbai, 400-005, India

Jian Zheng
Department of Modern Physics, University of Science and Technology of China, Hefei, Anhui 230026, People's Republic of China
(Received 6 February 2009; published 3 February 2010)

We present direct measurements of the absolute energy distribution of relativistic electrons generated in intense, femtosecond laser interaction with a solid. Cherenkov emission radiated by these electrons in a novel prism target is spectrally dispersed to obtain yield and energy distribution of electrons simultaneously. A crucial advance is the observation of high density electron current as predicted by particle simulations and its transport as it happens inside the target. In addition, the strong sheath potential present at the rear side of the target is inferred from a comparison of the electron spectra derived from Cherenkov light observation with that from a magnet spectrometer.

DOI: 10.1103/PhysRevLett.104.055001 PACS numbers: 52.38.−r, 52.59.−f, 52.70.Kz

Rapid progress of ultraintense laser (UIL) technology offers us novel ways of exploring high energy density physics [1]. The interaction of UIL with a solid creates relativistic electrons whose current is nearly 100 times stronger than that in lightning. Such extremely high energy density promises exciting applications such as laboratory astrophysics, particle acceleration, and the fast ignition (FI) of inertial fusion [2]. Given this significance, there is a compelling necessity for direct measurement of the high currents. However, this measurement has not been successful because of the fundamental and configurational difficulties faced by existing techniques; for example, the electron distribution outside the target is modified by giant self-excited electric and magnetic fields at target boundaries [3]. For these reasons, the observation of fast electron distribution inside the target is definitely required.

Cherenkov radiation is emitted when a charged particle passes through a dielectric material with a velocity larger than the speed of light, i.e., $v_e > c/n$, where n is the refractive index of the material. This radiation has (a) a unique emission angle depending on particle energy and refractive index of the material and (b) a threshold energy (velocity) for the emission [4,5]. Previous Cherenkov experiments using a planar target [6,7] could not obtain the exact energy spectrum of the electrons without support from numerical models or simulations because of (i) the need to account for interfering emissions such as transition radiation [8] or $K\alpha$ x-ray emission [9] and (ii) exclusion of overlapping of the signal due to electron refluxing at the rear surface of the target [10].

In addition, the use of planar targets (a) needs *a priori* assumption of the type of energy distribution (for example, exponential or relativistic Maxwellian), (b) must take into account loss of Cherenkov emission at large angles by total reflection, and (c) must address complications in the analysis due to refraction. The total reflection of Cherenkov light with larger emission angle corresponding to high energy particles, at the rear boundary of the planar target, can imply the loss of the higher energy part of the distribution.

We developed a novel prism target to resolve energy spectrum by avoiding not only the overlap of the characteristic ring pattern of Cherenkov radiation from electrons of different energies but also interference from other emissions such as transition radiation. Figure 1 shows a schematic image of the prism target. When the laser irradiates a thin tip of a dielectric target, the accelerated electrons emit optical Cherenkov radiation in a conical shape along the electron propagation axis. If the target is transparent for visible light, the emission inside the material is reflected at the oblique back surface to the bottom. The Cherenkov light in a certain direction has a different reflection angle, and this light appears at a distinct position on the bottom without any overlap with the light emitted at other angles. Therefore the light intensity of the observed image at the bottom can be converted into the electron energy distribution with absolute number. The bottom has a frosted surface as a screen in order to avoid angle-dependent partial reflection at the bottom. The image has a horseshoe pattern (a part of ellipse shape) as shown in Fig. 1(b) due to the reflection of the ring pattern of Cherenkov radiation.

Because electrons emit the Cherenkov radiation continuously during the propagation, the spatial separation at the bottom surface of the Cherenkov rays with different emission angle must be larger than electron travel distance in order to avoid overlapping. For this purpose, we attach a larger prism to the interaction prism target by optical contact technique to obtain a wider observation area as in Fig. 1(a). We choose BK7 as the prism material. The

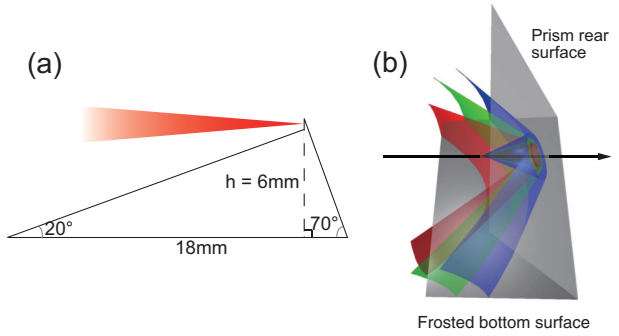

FIG. 1 (color). Schematic image of prism target. (a) Side view of the actual prism target geometry. Ultraintense laser (UIL) light irradiates a thin tip of the prism surface at near normal incidence. The fast electrons accelerated along the laser direction emit Cherenkov light, which is then reflected at the rear surface of the target and is scattered at the frosted bottom surface. (b) Bird's eye view of the prism target with Cherenkov light emitted from different energy electrons. Black arrow indicates the electron propagation direction (same with laser axis). Higher energy electrons emit larger angle Cherenkov light (blue) compared with middle (green) and lower (red) one in a conical shape. Because of the reflection at the rear surface, the observed image at the bottom becomes a horseshoe pattern as a part of the ellipse shape.

interaction surface of prism target is covered with an 11 μm aluminum coating for efficient generation of fast electrons. A 1 μm Al is overcoated on the larger prism surface under laser incident path to cut the noise on the bottom surface created in laser interaction. Al coating is also applied on the rear surface of target to enhance the light reflection.

Cherenkov light intensity is generally stronger at a shorter wavelength, so that UV light, which can propagate in glass without internal absorption, is commonly used in many experiments; namely, the light intensity has a peak at 350 nm for BK7 and 200 nm for quartz. The value of refractive index changes rapidly at shorter wavelengths, and therefore it is necessary to use a very narrow bandpass filter to reduce the blurring of the observed image because Cherenkov emission angle depends on the refractive index. On the other hand, at longer wavelengths (say, near 600 nm) the refractive index is relatively constant. In addition, Cherenkov light intensity at this wavelength is just $\frac{1}{2}$ to $\frac{1}{3}$ of that in the UV region. Based on these considerations, we chose to observe a wide range wavelength region (550–750 nm) rather than a narrow region in UV.

It is well known that the fast electron beam generated in UIL-plasma interaction has a considerable divergence, typically 30°–40° in FWHM [9,11]. This may cause a significant blurring of the observed Cherenkov image at the bottom. However, because the observable electron energy for BK7 prism is over about 200 keV, such high energy electrons may have a smaller divergence angle [12–14]. Furthermore, the emission angle of Cherenkov radiation defined as

$$\theta = \cos^{-1}\frac{1}{n(\lambda)\beta}, \quad (1)$$

indicates that the angle θ can saturate at higher electron energies (over a few MeV) because $\beta \simeq 1$. This feature appears as a clear edge on the outer ring of the Cherenkov image, and is even advantageous that one could estimate the fast electron divergence angle from the blur of the outer edge. The above two features indicate that high energy electrons, important for applications such as FI and nuclear reactions, can be selectively measured by the detection of their Cherenkov emission.

The experiment was conducted with a 20 TW/30 fs Ti: sapphire laser system at Tata Institute of Fundamental Research, Mumbai, India. The laser energy is 290 mJ on target with a 10 μm diameter focal spot diameter via an $f/3$ off-axis parabolic mirror, giving a maximum focal intensity of 9.2×10^{18} W/cm^2. As shown in Fig. 1, the laser light irradiates the edge of the prism target at near normal incidence where the 30 μm electron propagation length is expected. This distance is determined to have a good balance between enhancing the Cherenkov emissions and limiting other emissions, while simultaneously minimizing the electron scattering which could affect the observed image. The Cherenkov light at the frosted surface of the prism target is detected using an intensified charge coupled device (ICCD) camera. The light is collected through 2 achromatic lenses with 0.22× magnification, resulting in a spatial resolution of 58 μm and a viewing area of 6 cm × 6 cm. A bandpass filter (575–750 nm) with 80% transmission is placed in front of ICCD. As a comparison with Cherenkov observation, the energy spectrum of the electrons exiting the target is also observed with a magnet electron spectrometer (ESM) at 55 cm behind the target placed along the laser axis. The detectable electron energy range is from 0.1 to 7.3 MeV. This spectrometer has been absolutely calibrated [15].

A typical image taken at the bottom surface shows a clear horseshoe shape as shown in Fig. 2(a). The laser direction is from the left to the right and the pattern is symmetric to the propagation axis. The intense region (represented in red) close to the left center of this image is spread out in the vertical direction rather than the horizontal, so that we converted the vertical line shape, which is in left side on the figure, into the energy spectrum with a finer resolution. On the other hand, the beam divergence can be estimated from the blur on the vertical line shape due to the low spectral dispersion here. For this purpose, we performed a ray-trace calculation using an exact prism geometry giving an initial electron energy distribution. Figure 2(b) shows the horizontal line shapes of the horizontal center of horseshoe pattern in Fig. 2(a) with calculations. When the divergence is assumed to be perfect, we found that the no calculation results can be fitted to the outer edge of the experimental data. We found the different electron energy distribution changes only the inner line shape of the pattern (corresponding to left side of the peak).

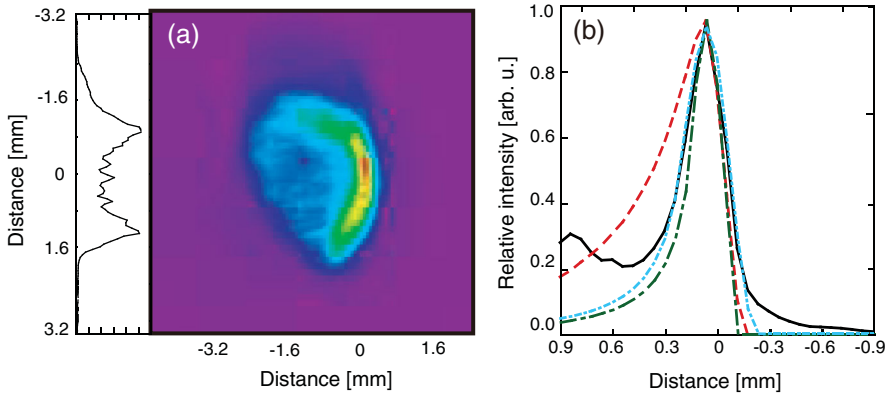

FIG. 2 (color). (a) Typical experimental result observed at the frosted bottom surface of prism target with ICCD. The left lineout is the vertical line profiles near the center of the figure. (b) The horizontal line profile from the experiment (solid line) and ray-trace calculations. Each calculation line represents an exponential distribution with a slope temperature of 0.2 MeV with no beam divergence (dashed line), 1.5 MeV with no divergence (dash-dotted line), and 1.5 MeV with 10° divergence (dotted line).

In the result, the line shape with 10° in FWHM best reproduces the experiment. (The electron distribution is assumed to be an exponential distribution with a slope temperature of 1.5 MeV, over where the line profile is not changed.) This angle may look relatively small compared to $K\alpha$ or other measurements that account for the divergence of keV electrons [9]. However, similar results have been observed in experiments in MeV range [16,17].

The electron energy spectrum converted from the horizontal line shape is plotted as open circles in Fig. 3. The number of electrons in each energy bins, $N(E)$, simply calculated from the light intensity in different positions of the Cherenkov pattern, given $N(E) = I_{\text{observed}}(x)/[N_{\text{Cherenkov}}(E)\ SR_{\text{Cherenkov}}(x)\ Q_{\text{ICCD}}\ G_{\text{ICCD}}\ T_{\text{optics}}\ SR_{\text{col}}]$, where E is the electron energy as a function x, $I_{\text{observed}}(x)$ is the observed Cherenkov light intensity at each position, $N_{\text{Cherenkov}}(E)$ the emission efficiency per single electron, $SR_{\text{Cherenkov}}(x)$ the ratio of Cherenkov light to be delivered into spatial resolved area in the bottom screen, Q_{ICCD} the quantum efficiency of ICCD, T_{optics} the transmittance of optics, G_{ICCD} the gain of the ICCD, SR_{col} the solid angle of the scattered light on the screen via collection lens. As a comparison, the electron spectra from the magnet spectrometer (open square) and one-dimensional particle-in-cell (PIC) simulations (solid triangles) [18] are also plotted. The simulation condition is taken from the experimental parameters and a plasma scale length of 0.1 μm is assumed in front of solid density Al plasma layer. The spectrum is taken at the maximum laser absorption (after 40 fs from the starting of laser injection) in which the total electron energy exceeds 30% of the laser energy. One can easily see a large discrepancy between the PIC simulation and the magnet spectrometer measurements. This is due to self-generated fields at target rear retarding escaping electrons [3]. On the other hand, the raw Cherenkov spectrum indicates about 20 times higher flux than the one by the magnet spectrometer, but 10 times smaller than typical PIC result.

Because of the strong current, the target is easily ionized by electrostatic field ahead of the beam without increase of material temperature. Since Cherenkov radiation is emitted when the condition that electron velocity is larger than c/n is satisfied, it is no longer emitted from plasma after ionization. Conversely, we can estimate how many electrons contribute to Cherenkov emission by knowing the speed of ionization front along the electron propagation. The speed of ionization front is a function of current density as per detailed analyses [19,20]. Consequently, the electron number and ionization speed can be uniquely determined from the experimental Cherenkov light intensity. Using the numerical model in Ref. [20], we derived the total electron spectrum as shown by solid circles in Fig. 3 and estimate the ionization speed of 0.8 c. Clearly, the recovered electron spectrum is in excellent agreement with the PIC result.

In the above discussions we assumed a one-dimensional geometry of ionization front. In reality, only the center part of the electron beam might ionize the target while the outer part heats the target, so that Cherenkov light could be continuously emitted from the heated region. One may point out that such heated regions might complicate the analysis of the obtained Cherenkov pattern since the refractive index is generally a function of temperature. However, this dependence is small enough, typically of the order of 10^{-6} dn/dT, until the temperature reaches melting point (820 K) compared with the difference of the refractive index between 550 to 770 nm (nearly 0.5%). In addition, even if the state of solid material is changed to liquid or gas, their refractive indices are generally smaller than that of the solid. As a result, the emission angle of Cherenkov radiation reduces and comes close to the left side in Fig. 2(a). From this consideration, we rule out the effect of temperature in the experimental results.

The electrons escaping from the target suffer the self-created sheath potential at the rear surface. The electrons detected with ESM pass through the potential, resulting in reduction of their energies according to the strength of the potential. Comparing with the recovered spectrum, the ESM spectrum is downshifted by 500 keV with similar decay line form. This energy is nearly equivalent with the average energy of recovered electrons if the lower energy part of the recovered spectrum is similar with the PIC spectrum. This fact represents the important possibility that the formation of strong sheath field at the target boundary of which strength is equivalent with the average

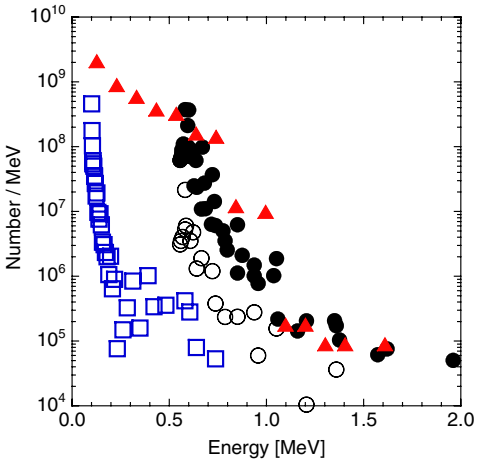

FIG. 3 (color online). Electron spectra converted directly from the horizontal line shape of Fig. 2(a) (open circles) and the inferred spectra (solid circles). Typical error in the horizontal axis is about 30% due to uncertainties of origin point. Error in vertical axis is about $\pm 10\%$ arising from the uncertainty of electron number below 500 keV. The spectra taken with a magnet spectrometer and from a 1D-PIC simulation with scale length of 0.1 μm are also shown as open squares and solid triangles, respectively. The PIC scale length is expected from the observed contrast ratio ($<3 \times 10^{-6}$ in ns and $<1.4 \times 10^{-5}$ in ps range).

energy of fast electrons inside the target as predicted from the results of ion acceleration [21]. In fact, in the above PIC calculation, the maximum potential at the rear side is a few hundred keV.

In conclusion, we conducted an experiment on fast electron energy transport using a novel prism target to obtain an absolute, *in situ* measurement of the fast electrons via Cherenkov emission. The crucial advance we put forth is the measurement of the electron characteristics in actual transport, without modifications by the dominant electric and magnetic fields that exist at the target boundaries. The obtained electron spectrum shows an excellent agreement with the PIC calculation using actual experimental parameters. This clearly demonstrates that the energy conversion of fast electrons can be as large as a few tens of percent of laser energy as predicted by the simulations. Comparing both spectra of the Cherenkov origin and the ESM appears an formation of strong sheath potential of which strength is determined by the average energy of the fast electrons inside the target. The existence of extreme high energy density current will potentially open up tantalizing applications in the area of high energy density science [22].

This work was fully supported by the international collaboration program of the Japan Society for the Promotion of Science (JSPS) and the Indian National Science Academy (INSA). A part of the instruments is supported by a Grant-in-Aid for Scientific Research of JSPS (Contract No. 19206099). G. R. K. acknowledges an ORI grant from DAE-SRC, Government of India. A part of the research is also supported by the JSPS-CUP (Core University Program) in the fusion area operated by NIFS (National Institute of Fusion and Sceince). The authors gratefully acknowledge Professor H. Sakagami, National Institute for Fusion Science, Japan, for his permission to use his 1D-PIC code.

*Present address: Laboratoire d'Optique Appliquée, Ecole Polytechnique, ENSTA, CNRS, UMR 7639, 91761 Palaiseau, France.

[1] *Frontiers in High Energy Density Physics: The X-Games of Contemporary Science*, edited by the Committee on High Energy Density Plasma Physics (National Academies Press, Washington, DC, 2003).
[2] M. Tabak, J. Hammer, M. E. Glinsky, W. L. Kruer, and S. C. Wilks, Phys. Plasmas **1**, 1626 (1994).
[3] T. Yabuuchi *et al.*, Phys. Plasmas **14**, 040706 (2007); **10**, 2009 (2003).
[4] J. D. Jackson, *Classical Electrodynamics* (John Wiley & Sons. Inc., New York, 1975), 2nd ed.
[5] J. Zheng, C. X. Yu, Z. J. Zheng, and K. A. Tanaka, Phys. Plasmas **12**, 093105 (2005).
[6] F. Brandl, G. Pretzler, D. Habs, and E. Fill, Europhys. Lett. **61**, 632 (2003).
[7] M. Manclossi *et al.*, Phys. Rev. Lett. **96**, 125002 (2006).
[8] J. Zheng *et al.*, Phys. Rev. Lett. **92**, 165001 (2004).
[9] R. B. Stephens *et al.*, Phys. Rev. E **69**, 066414 (2004).
[10] Y. Sentoku, T. E. Cowan, A. Kemp, and H. Ruhl, Phys. Plasmas **10**, 2009 (2003).
[11] R. Kodama, P. A. Norreys, K. Mima, A. E. Dangor, and R. G. Evans *et al.*, Nature (London) **412**, 798 (2001).
[12] Y. T. Li *et al.*, Phys. Rev. E **69**, 036405 (2004).
[13] L. Gremillet *et al.*, Phys. Rev. Lett. **83**, 5015 (1999).
[14] M. Borghesi *et al.*, Phys. Rev. Lett. **83**, 4309 (1999).
[15] K. A. Tanaka *et al.*, Rev. Sci. Instrum. **76**, 013507 (2005).
[16] C. Gahn, G. D. Tsakiris, A. Pukhov, J. Meyer-ter-Vehn, G. Pretzler, P. Thirolf, D. Habs, and K. J. Witte, Phys. Rev. Lett. **83**, 4772 (1999).
[17] G. Malka *et al.*, Phys. Rev. E **66**, 066402 (2002).
[18] H. Sakagami and K. Mima, in *Proceedings of the of Second International Conference on Inertial Fusion Sciences and Applications, Kyoto, 2001* (Elsevier, New York, 2002), pp. 380–383.
[19] S. I. Krasheninnikov, A. V. Kim, B. K. Frolov, and R. Stephens, Phys. Plasmas **12**, 073105 (2005).
[20] O. Klimo, V. T. Tikhonchuk, and A. Debayle, Phys. Rev. E **75**, 016403 (2007).
[21] S. P. Hatchett *et al.*, Phys. Plasmas **7**, 2076 (2000).
[22] R. Kodama *et al.*, Nature (London) **432**, 1005 (2004).